Int. J. Electrochem. Sci., 7 **(2012)** 3737 - 3749

International Journal of ELECTROCHEMICAL SCIENCE
www.electrochemsci.org

Neural Network Predictive Control of a SOFC Fuelled with Ammonia

S. A. Hajimolana, M. A. Hussain[*]*, W. M. A. Wan Daud, M. H. Chakrabarti*

Chemical Engineering Department, Faculty of Engineering, University of Malaya, 50603, Kuala Lumpur, Malaysia.
[*]E-mail: mohd_azlan@um.edu.my

Received: 31 January 2012 / *Accepted:* 6 March 2012 / *Published:* 1 April 2012

The dynamic behavior and control of a tubular solid oxide fuel cell will be studied in this paper. The effect of fuel/air temperature and pressure will be investigated. Controlling the average stack temperature is the final objective of this study due to a high operating temperature of the system. In this case, temperature fluctuation induces thermal stress in the electrodes and electrolyte ceramics; therefore, the cell temperature distribution should be kept as constant as possible. A mathematical modeling based on first principles is developed. The fuel cell is divided into five subsystems and the factors such as mass/energy/momentum transfer, diffusion through porous media, electrochemical reactions, and polarization losses inside the subsystems are presented. Dynamic fuel-cell-tube temperature responses of the cell to step changes in conditions of the feed streams will be presented. A neural network predictive controller (NNPC) is then implemented to control the cell-tube temperature through manipulation of the temperature of the inlet air stream. The results show that the control system can successfully reject unmeasured step changes (disturbances) in the load resistance.

Keywords: ammonia fuel, neural network predictive control, SOFC, cell-tube temperature.

1. INTRODUCTION

Solid oxide fuel cells (SOFCs) have shown promise in the electricity generating sector for stationary applications in the mid-term future. This is due to the fact that the energy efficiency usually achieved in a SOFC is much greater than that obtained from conventional heat engines or any other types of fuel cells. SOFCs offer high power density, low cost, scalability, fuel flexibility, and superior durability. Although much experimental work has been done on ammonia-fuelled solid oxide fuel cells (NH_3-SOFCs) [2; 9-11; 17; 24], only few research studies are available on mathematical modeling of the NH_3-SOFC [12-15]. Also the experimental data reported in the literature doesn't give full details

of the design parameters such as fuel cell lengths, diameters, etc. As a result, it is not easy to validate experimental results by means of mathematical modeling. Thus model validation is first performed using H_2-SOFCs before performing a full simulation on NH_3-SOFCs [15].

Besides working on fuel cell modeling, several well established Model Predictive Control (MPC) methods are available in the literature [5-7; 23; 26-28; 32]. MPC is a powerful modern process control methodology. Wu et al. [25] used a predictive controller based on a T–S fuzzy model to maintain the stack temperature. Vijay et al. [22] proposed a predictive controller based on a bond graph SOFC model. The control objective was achieved by adjusting four air and fuel inlet and outlet valves. It was observed that the control objectives involving the constrains on the fuel utilization, air utilization, the cell operating temperature and the anode and cathode pressure could control by the proposed control system. Li et al. [8] proposed a nonlinear MPC methodology based on genetic optimization to keep the fuel cell voltage and fuel utilization at desired values. Their model was a simple nonlinear model mainly representing the electrochemical process. They showed that in the presence of a +13% load change, the closed-loop performance was satisfactory.

In this work, the objective is to control the fuel cell temperature using a neural network predictive control (NNPC) that manipulates the inlet air flow temperature. Such a control study for SOFCs has not been reported in the literature. Our previous model [4] is used for the controller design.

2. MODEL DESCRIPTION

The mathematical model used in this study was adapted from a model reported earlier [4]. The SOFC system under study here is a bank of single tubular SOFCs. Each cell has two tubes, an outer and an inner tube, as shown in Fig. 1. The outer one is a cell tube. The outer surface of the outer tube is the anodic side of the cell and its inner surface is the cathodic side. Between the anodic and cathodic sides (surfaces) lies the solid oxide electrolyte. The inner tube is an air injection tube and composed of alumina, from which preheated air is injected into the bottom of the cell tube and flows over the cathode surface through the gap between the injection tube and the cell tube. Fuel gas flows over the anode surface through the gap among the cell tubes.

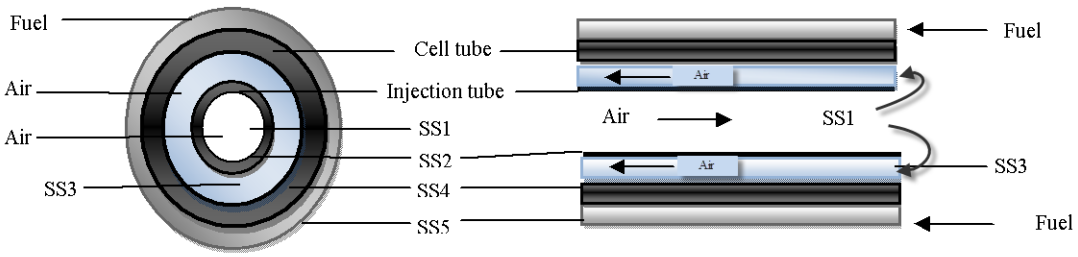

Figure 1. Division of the single tubular SOFC into five subsystems.

To develop a first-principles model of the SOFC system, a single tubular fuel cell is considered and divided into five subsystems (see Fig. 1):

- Subsystem 1 (SS1): air inside the injection tube;
- Subsystem 2 (SS2): solid injection tube;
- Subsystem 3 (SS3): air inside the space between the cell and injection tubes;
- Subsystem 4 (SS4): cell tube; and
- Subsystem 5 (SS5): fuel flow channel.

The fuel cell model is derived by writing mass, energy and/or momentum conservation equations for each of the five subsystems. Tables 1 and 2 present the parameters used in the simulation and operating conditions, respectively. The assumption considered in the mathematical formulation is that the gas boundary layers are very small relative to the corresponding radius; therefore, the equations governing the diffusion processes are written in Cartesian coordinates. Fluid velocities, temperatures and pressures are averaged along the radial direction. Specific properties such as conductivities, heat capacities, viscosities and densities in each subsystem are also uniform. Furthermore, output partial pressures, temperatures and velocities are equal to the pressures, temperatures and velocities inside the subsystem. The external load (load impedance) of the cell is a pure resistance.

Table 1. Parameters used in simulation.

Parameter	Value	Reference
A_{ano}	1.5×10^{-4} m^2	
r_{cto}	1.2×10^{-3} m	[20]
r_{cti}	1.1×10^{-3} m	[20]
r_{ito}	7.5×10^{-4} m	[20]
r_{iti}	7×10^{-4} m	[20]
L	2.5×10^{-1} m	[20]
m_{ct}	4.317×10^{-2} kg	
m_{it}	8.735×10^{-3} kg	
C_{ct}	3×10^{-1}	[29]
R_{tct}	9×10^{-1}	[29]
R_{to}	1×10^{-1}	[29]
z_r	3.325×10^{12}	[29]
E_r	1.962×10^{5}	[29]
$\tilde{C}_{p_{ct}}$	7.4×10^{-1}	[29]
$\tilde{C}_{p_{it}}$	$0.9768 + 0.000241\times T_{it}$ kJ/(kg K)	[29]
ε_{cat}	4×10^{-1}	[20]
τ_{cat}	5	[20]
ε_{ano}	4×10^{-1}	[20]
τ_{ano}	5	[20]
Δ_{ano}	5×10^{-5}	[20]
Δ_{cat}	1.3×10^{-4}	[20]
$E_{act_{ano}}$	1.1×10^{5}	[29]
$E_{act_{cat}}$	1.2×10^{5}	[29]

Table 2. Operating Conditions of the NH_3-SOFC model

Parameter	Value	Reference
R_{load}	4 Ω	[4]
$P^{ano}_{fuel_{in}}$	1 atm	[20]
$T^{ano}_{fuel_{in}}$	1023	[20]
$u^{ano}_{fuel_{in}}$	6.42 m/s	
$\overline{\xi}^{ano}_{NH_{3in}}$	0.939	[13]
$\overline{\xi}^{ano}_{H_{2in}}$	0.03	[13]
$\overline{\xi}^{ano}_{N_{2in}}$	0.001	[13]
$\overline{\xi}^{ano}_{H_2O_{in}}$	0.03	[13]
$\overline{\xi}^{ano}_{O_{2in}}$	0.2333	[13]
$P^{inj}_{air_{in}}$	1 atm	[20]
$T^{inj}_{air_{in}}$	1173 K	[20]
$u^{inj}_{air_{in}}$	450 m/s	

The mass/momentum and energy balance inside SS1, SS3 and SS5 are given as follows, respectively:

$$L\frac{d\xi^i_j\rho^i_j}{dt} = u^i_{j_{in}}\xi^i_j\rho^i_{j_{in}} - u^i_j\xi^i_j\rho^i_j + \sum N_j M_j\left(\frac{2r_iL}{r^2_i - r^2_0}\right) + nr_j \tag{1}$$

$$L\frac{d(u_i\rho_i)}{dt} = (u_{i_{in}})^2\rho_{i_{in}} - (u_i)^2\rho_i + \frac{\rho_{i_{in}}R^*T_{i_{in}}}{M_i} - \frac{\rho_i R^*T_i}{M_i} \tag{2}$$

$$L\frac{d(\tilde{H}^i_j\rho^i_j)}{\partial t} = \rho^i_{j_{in}}u^i_{j_{in}}H^i_{j_{in}} - u^i_j\rho^i_j\tilde{H}^i_j + \frac{2Lh_w}{r}\left(T_w - T^i_j\right) \tag{3}$$

where i is air flow injection tube, air flow inside cathode side, fuel flow inside anode side, j is air, oxygen, nitrogen, ammonia, hydrogen, w is the wall, N_j is mass transfer by means of diffusion, n is the molar number and r_j is producing or consuming of the components.

This model assumes that the pressure drop caused by the pipe resistance over the distance L is negligible. It is also assumed that energy is transferred to the flow streams by convection only.

Enthalpy of formation, heat capacities, viscosities, and conductivities of the components of air and the fuel are given in a previous work [4].

Energy balance for the solid parts (SS2 and SS4) leads to:

$$m_s \tilde{C}_{p_s} \frac{dT_s}{dt} = \frac{\sigma 2\pi rL}{R_{rad}}\left(T_w^4 - T_j^4\right) + 2\pi rLh_w(T_j^i - T_w) + 2\pi rLh_w\left(T_j^i - T_w\right) + \sum H_j N_j \begin{pmatrix} 2r & L \\ i & \\ r^2 - r^2 & \\ i & 0 \end{pmatrix} + \quad (4)$$

$$2r_{ct_o} LR_{NH_3} \Delta H_{R_{NH3}} - 0.001 V_{out} I$$

The last three parts are heating transfer by means of diffusion, heating consuming by ammonia decomposition and heating supply by electrochemical reaction, respectively only in SS4.

Electrochemical reaction occurs inside the fuel cell at the triple phase boundary (TPB), which as a result produces voltage and current. At the cathodic side oxygen ions (with a negative charge) migrate through the crystal lattice. H_2 in the fuel stream diffuses into the anodic side and reacts at the TPB with oxide ions (O^{2-}) from the electrolyte to produce water. The electrons pass outside the fuel cell, through the load, and back to the cathode, where oxygen from the air receives the electrons and is converted to oxide ions, which are then injected into the electrolyte. The SOFC electrochemical reactions that occur inside the TPB are [33]:

$$Anodic\ \ Side\ \ \text{Re}action \left\{ H_2 + O^{2-} \longrightarrow H_2O + 2e \right\}$$

$$Cathodic\ \ Side\ \ \text{Re}action \left\{ O_2(g) + 4e \longrightarrow 2O^{2-} \right\}$$

The Nernst potential for these reactions is given by:

$$E_{H_2} = E_{H_2}^0 + \frac{R_J T_{ct}}{2F} \ln\left[\frac{P_{H_2}^{TPB} (P_{O_2}^{TPB})^{1/2}}{P_{H_2O}^{TPB}} \right] \quad (5)$$

However, the actual cell voltage (E) is less than its theoretical open circuit voltage because it is strongly affected by several irreversible losses including activation losses due to irreversibility of electrochemical reactions at the three-phase boundary (TPB), concentration losses due to mass transport resistance in the electrodes (especially for thick anodes as in an anodic-supported SOFC) and ohmic losses due to ionic and electronic charge transfer resistances. Actual voltage is thus given by:

$$E = E_{H_2} - \eta_{act_{H_2}} - \eta_{conc_{H_2}} - \eta_{act_{O_2}} - \eta_{conc_{O_2}} - \eta_{ohm} \quad (6)$$

The activation polarizations are the result of the kinetics involved with the electrochemical reactions. It becomes an important loss when the current is low, because at low currents the reactants

must overcome an energy barrier named activation energy (E_{act}) to drive the electrochemical reactions at the electrode-electrolyte interface and this barrier leads to the polarization. The activation barrier is the result of many complex electrochemical reaction steps where, typically, the rate-limiting step is responsible for the polarization. One can account for the anodic and cathodic activation polarizations using the Butler-Volmer correlation [30]:

$$\eta_{act_{ano}} = \frac{R_J T_{ct}}{F} \sinh^{-1}\left(\frac{I}{2I_{0_{ano}}}\right) \tag{7}$$

$$\eta_{act_{cat}} = \frac{R_J T_{ct}}{F} \sinh^{-1}\left(\frac{I}{2I_{0_{cat}}}\right) \tag{8}$$

where I_{0ano} and I_{0cat} are the anodic and cathodic exchange currents, respectively, which are given by (Campanari and Iora, 2004):

$$I_{0_{ano}} = 14\times10^{9}\pi r_{ct_o} L\left(P_{H_2}^{TPB}\right)\exp\left(\frac{E_{act_{ano}}}{R_{kJ}T_{ct}}\right) \tag{9}$$

$$I_{0_{cat}} = 14\times10^{9}\pi r_{ct_i} L\left(P_{O_2}^{TPB}\right)^{1/4}\exp\left(\frac{E_{act_{cat}}}{R_{kJ}T_{ct}}\right) \tag{10}$$

Concentration losses are those associated with concentration variation of the critical species due to mass transport processes. There are usually two sources of losses that are due to mass transport: (i) diffusion between the bulk phase and cell surfaces, and (ii) transport of reactants and products through electrodes. Therefore, the concentration polarization is highly dependent on the gases used, as well as the distance through which the gases must diffuse. Pore volume percentage, as well as diffusion length, can be varied to optimize these properties. For similar geometries, cathodic concentrations are much larger than anodic concentrations, because of the lower diffusivities of O_2/N_2 in the cathode than H_2/H_2O in the anode. The anodic and cathodic concentration losses can be calculated respectively as follows [3]:

$$\eta_{conc_{H_2}} = \frac{R_J T_{ct}}{2F} \ln\left(\frac{P_{H_2} P_{H_2O}^{TPB}}{P_{H_2}^{TPB} P_{H_2O}}\right) \tag{11}$$

$$\eta_{conc_{O_2}} = \frac{R_J T_{ct}}{4F} \ln\left(\frac{P_{O_2}}{P_{O_2}^{TPB}}\right) \tag{12}$$

An approximate equivalent circuit of an SOFC that consists of two internal resistances and one internal capacitance can be found in another work [18]. According to the equivalent circuit approximation, the cell output voltage is governed by

$$\frac{dV_{tl}}{dt} = \left(\frac{1}{R_{tct}C_{ct}}\right)E - \frac{1}{C_{ct}}\left(\frac{1}{R_{tct}} + \frac{1}{R_{to}+R_{load}}\right)V_{tl} \tag{13}$$

$$V_{out} = \left(\frac{R_{load}}{R_{to}+R_{load}}\right)V_{tl}$$

$$I = \left(\frac{1}{R_{to}+R_{load}}\right)V_{tl}$$

where R_{to} is the total ohmic resistance in the inherent impedance of the cell, R_{tct} is the total charge transfer resistance of the cell, C_{ct} is the charge transfer capacitance of the cell, I is the current through the external resistive load, V_{out} is the fuel cell output voltage (voltage across the external load) and V_{tl} is the voltage across the total ohmic resistance and the load resistance in series.

The thermal decomposition of ammonia for hydrogen production in the porous anode is solved using the chemical model described as follows. NH_3 thermal decomposition takes place on the anode surface (fuel) channel (SS4) as this process is favored at high temperatures. In the present study, it is considered that thermal decomposition can take place in the composite anode of the SOFC with typical catalyst (Ni) loading [14]:

$$r_{NH_3} = z_r \exp\left(-\frac{E_r}{R_{kj}T_{ct}}\right)P_{NH_3} \tag{14}$$

where P_{NH3} is the partial pressure of NH_3. It is considered that the reaction rate is mainly dependent on the partial pressure of NH_3 and the operating temperature. It is assumed here that NH_3, H_2O and N_2 diffuse into the anode at a negligible rate; only H_2 gas diffuses into the anode (subsystem 4)

3. RESULTS AND DISCUSSION

3.1. Model validation

Simulation was done to compare the results with the experimental data of Singhal [20]. In this simulation, the values of fuel and airflow rates were adjusted to match the values of factors given by Singhal [20]. The current–potential plot obtained from this simulation was compared with the experimental data and the predictions from the model developed by Ota and co-workers [16], as shown

in Fig. 2. Excellent agreement was obtained in the low current density region in comparison to the model developed by Ota et al.[16], which actually showed some deviation from experimental results. After validating the mathematical model developed in this work with experimental results of Singhal [20] for H_2-SOFC, the model was improved to account for NH_3-SOFC.

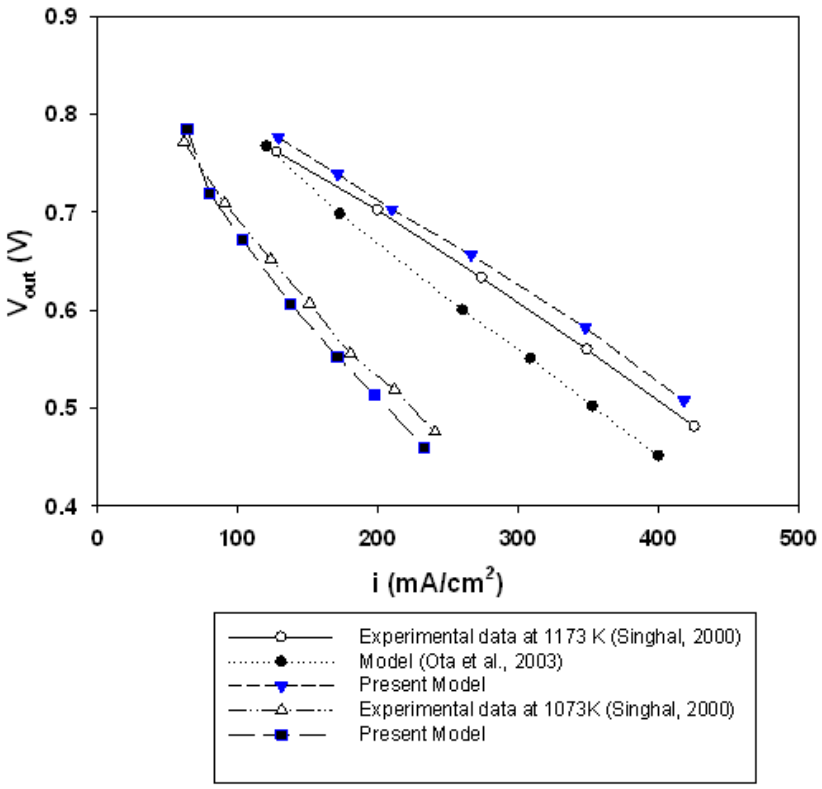

Figure 2. Comparison of current–potential plots from the present model, model from Ota et al. (2003) and the experimental data available in the literature (Singhal, 2000).

3.2. Open-loop Dynamic Cell Responses

The dynamic model of the SOFC system derived in the previous section has 20 first order ordinary differential equations, which are integrated numerically using MATLAB. Figure 3 and 4 depict the dynamic responses of the fuel cell to step changes of +5% in the temperature, pressure, and velocity of the inlet fuel and air stream respectively at time t= 100 s. The results of simulation indicate that the transient response of the SOFC is mainly controlled by the temperature dynamics. Simulation results also show that the temperature and pressure of the inlet air stream and the temperature of the inlet fuel stream strongly affect the fuel cell system. They also indicate that temperature of the inlet air stream has the strongest effect on the cell performance, and effects of the inlet air and fuel velocities on the cell response are weaker than those of inlet feed pressures and temperatures.

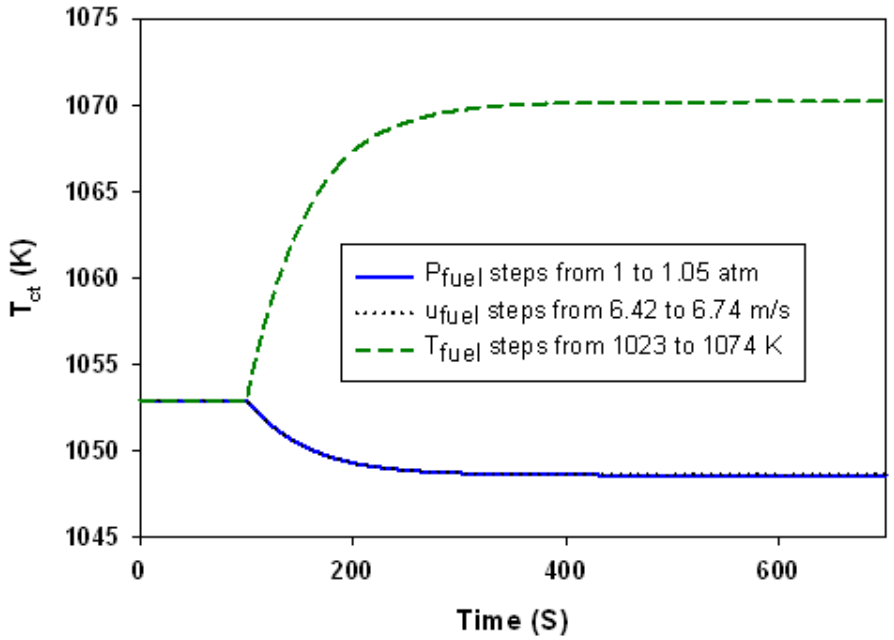

Figure 3. Open-loop responses of the SOFC to step changes of +5% in the inlet fuel stream

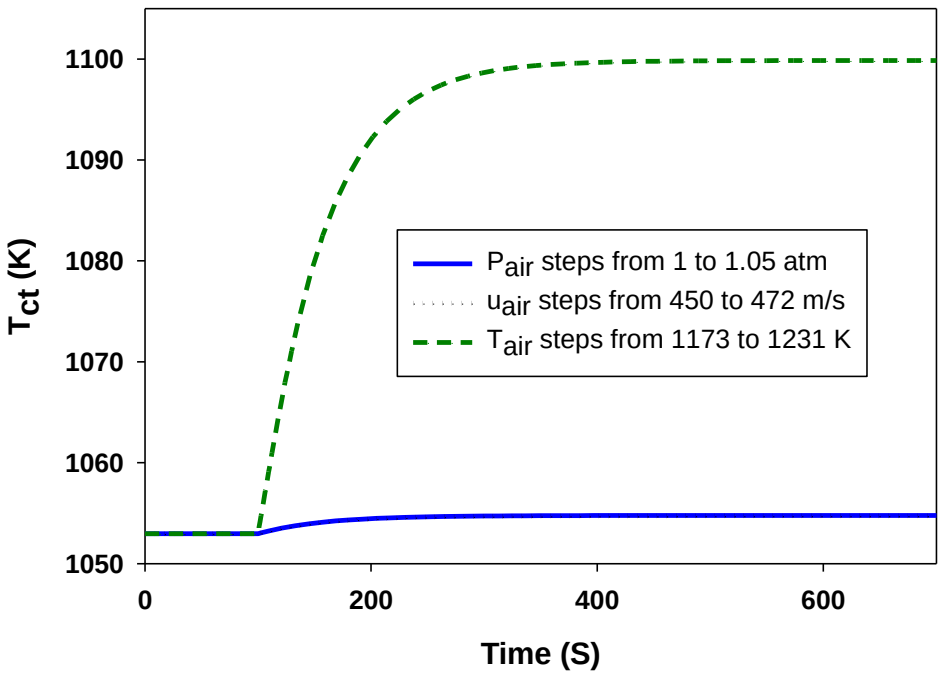

Figure 4. Open-loop responses of the SOFC to step changes of +5% in the inlet air stream

4. NEURAL NETWORK PREDICTIVE CONROL OF THE SOFC SYSTEM

A SOFC has a problem with regard to the durability of the ceramics used as its cell materials, because its operating temperature is very high, and its cell temperature fluctuation induces thermal

stress in the ceramics. Therefore, the cell temperature distribution should be kept as constant as possible. In this case, NNPC is used to predict future plant responses to control signals.

The first step in model predictive control is to establish the neural network plant model and prepare a neural network to characterize the forward dynamics of the plant. The estimated error between the plant output and the neural network output is employed as the neural network training signal. The neural network plant model uses earlier inputs and preceding plant outputs to estimate future values of the plant output.

The controller then estimates the input parameter that will optimize plant performance over a precise imminent time horizon [21].

$$J\left(k,u\left(k\right)\right)=\sum_{L=M_1}^{M_2}\left(\alpha_r(k+L)-\alpha_m(k+L)\right)^2+\gamma\sum_{L=1}^{M_u}\left(u(k+L-1)\right)^2 \tag{7}$$

where signals $\alpha_r(k+L)$, $\alpha_m(k+L)$,$u(k+j)$are the j-step predictions of the process output, the reference course and the control input, respectively. M_1 is the minimum costing scope, M_2 is the prediction scope (maximum costing scope), and M_u is the control scope and defines the horizons over which the tracking error and the control increments are determined. The u variable is the provisional control signal, α_r is the desired reaction, and α_m is the network model reaction. The parameter γ represents the weight of the control signal.

At each sampling stage, only the first control signal of the estimated sequence is applied to the controlled process. At the next sampling time the method is repeated. This is known as the receding horizon concept.

The controller consists of the plant model and the optimization block. Eq. (7) is used in a particular sequence with the input and output constraints [22]:

$$u_{min}\leq u\leq u_{max}$$

$$\Delta u_{min}\leq\Delta u\leq\Delta\, u_{max}$$

$$\alpha_{min}\leq y\leq y_{max}$$

$$\Delta\alpha_{min}\leq\Delta y\leq\Delta\, y_{max}$$

The ability to deal with constraints is one of the key properties of MBPC and also results in its spread, use, and popularity in industry. MBPC algorithms are known to be very versatile and robust in process control applications. This neural network model has three layers, input, hidden and output. In off-line training of the neural network, 10,000 input and output vector sets are generated, using the neural network predictive control Matlab toolbax. A total of 8000 of these are used as a learning set, while others are used as a testing set. The training process is completed in approximately1,100,000 iterations. The error at the end of the learning is 0.0072135 for the training set. After finishing the training the next process is implementing these data in the neural network predictive control.

For ensuring good performance of the NNPC, the tuning parameters must be at an appropriate level. Although the parameters are tuned as per the recommendation of Shridhar and Cooper [19] initially the exact values are fine tuned based on actual control performance. In addition to the selection of controller tuning parameters, appropriate values are chosen for input/output variable constraints and these are imposed on loops based on practical experience. The tuned variables for NNPC are listed in Table 3. The values of the upper and lower limits of the constraints for $1110\ K \leq T_{air} \leq 1250\ K$ and for the cell tube-temperature can be specified as 1000 K (minimum) and 1100 (maximum), respectively, while an output variables weight of 1 is used along with the manipulated variables weight of 0.1. The control system has a sampling time of 15 sec.

Table 3. Tuning parameters of NNPC

Tuning parameters	NNPC
Control interval (time units)	2
Prediction horizon (intervals)	5
Control horizon (intervals)	1

4.1. Closed-loop simulation result

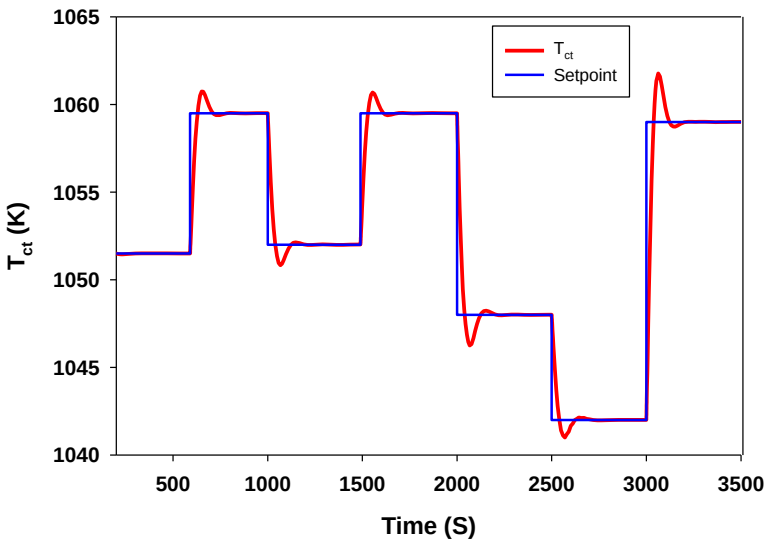

Figure 5. The performance of the NNPC in tracking series of set-point change in T_{ct}.

MPC refers to a class of control algorithms in which a dynamic model of the plant is used to predict and optimize the future behavior of the process. The basic control strategy of the MPC is to select a set of future control horizons and minimize a cost function based on the desired output

trajectory over a prediction horizon with a chosen length. To select the manipulated input that has the strongest effects (in terms of dimensionless steady-state gain) on the controlled output, the open-loop analysis suggests that the cell tube temperature can be paired with the air inlet temperature. Figure 5 shows the performance of the NNPC in tracking the series of setpoint changes for T_{ct}. The efficiency of the NNPC technique is demonstrated by the fact that the cell tube-temperature is driven to the trajectory rapidly and evenly. The controller responses show that the cell tube-temperature attains the required temperature set-points without fluctuation and seldom overshoots. Therefore, the NNPC is competent in controlling the SOFC cell tube-temperature. Furthermore, Fig. 6 demonstrates that the inlet air flow temperature control sequence for the aforementioned dynamic responses varies evenly. For example, the maximum value of inlet air flow temperature increase is lower than 1250 K.

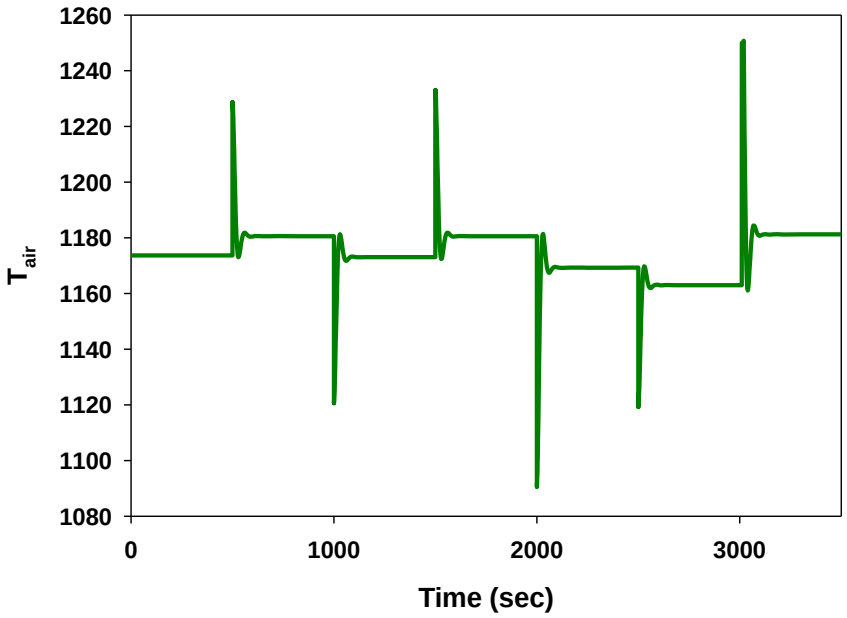

Figure 6. Manipulated variable profile corresponding to Figure 5.

4. CONCLUSION

A dynamic model of a tubular solid oxide fuel cell (SOFC) was presented. Simulation results indicate that temperature of the inlet air stream has the strongest effect on the cell performance. The cell-tube temperature was regulated effectively using a NNPC that manipulates the temperature of the inlet air stream. The performance of the control system was determined to be satisfactory to reject the unmeasured disturbances.

ACKNOWLEDGMENT
The authors are grateful to the University of Malaya Research Grant, UM/MOHE High Impact Research Grant No. UM.C/625/1/HIR/MOHE/ENG/18 and the UM Bright Sparks Unit Bsp_App462/11(K) for providing financial assistance for this project.

References

1. A.E. Auld, F. Mueller, K.M. Smedley, S. Samuelsen, and J. Brouwer. *J. Power Sources*, 179 (2008) 155.
2. G.G.M. Fournier, I.W. Cumming, and K. Hellgardt, High performance direct ammonia solid oxide fuel cell. *J. Power Sources*, 162 (2006) 198.
3. S.A. Hajimolana, M.A. Hussain, W.M.A.W. Daud, M. Soroush, and A. Shamiri, *Renew and Sustain Energ Rev*, 15 (2011) 1893.
4. S.A. Hajimolana, and M. Soroush, *Ind. Eng. Chem*, 48 (2009) 6112.
5. H.-B. Huo, Z.-D. Zhong, X.-J. Zhu, and H.-Y. Tu. *J. Power Sources*, 175 (2008) 441.
6. F. Jurado, *Energy*, 30 (2005) 1711.
7. F. Jurado, *J. Power Sources*, 158 (2006) 245.
8. Y. Li, J. Shen, and J. Lu. *J. Power Sources*, 196 5873.
9. Q. Ma, J. Ma, S. Zhou, R. Yan, J. Gao, and G. Meng. *J. Power Sources*, 164 (2007) 86.
10. N. Maffei, L. Pelletier, J.P. Charland, and A. McFarlan. *J. Power Sources*, 140 (2005) 264.
11. G. Meng, C. Jiang, J. Ma, Q. Ma, and X. Liu. *J.Power Sources*, 173 (2007) 189.
12. M. Ni. *Energ Conv. Manag*, 51 (2010) 714.
13. M. Ni. *Int. J. Hyd. Energ*., 36 (2011) 3153.
14. M. Ni, D.Y.C. Leung, and M.K.H. Leung. *J. Power Sources*, 183 (2008) 687.
15. M. Ni, D.Y.C. Leung, and M.K.H. Leung. *Int. J. Hyd. Energ.*, 33 (2008) 5765.
16. T. Ota, M. Koyama, C.-j. Wen, K. Yamada, and H. Takahashi. *J. Power Sources*, 118 (2003) 430.
17. L. Pelletier, A. McFarlan, and N. Maffei. *J. Power Sources*, 145 (2005) 262.
18. Y. Qi, B. Huang, and J. Luo. *Chem. Eng. Sci*. 61 (2006) 6057.
19. R. Shridhar, and D.J. Cooper. *Ind. Eng. Chemi. Res*., 36 (1997) 729.
20. S.C. Singhal. Solid State Ion, 135 (2000) 305.
21. A. Vasičkaninová, and M. Bakošová. *Acta Chimica Slovaca* 2 (2009) 21.
22. P. Vijay, A.K. Samantaray, and A. Mukherjee. *Mechatronics* 19 (2009) 489.
23. X. Wang, B. Huang, and T. Chen. *J. Proc. Contr*.,17 (2007) 103.
24. A. Wojcik, H. Middleton, I. Damopoulos, and J. Van herle. *J. Power Sources*, 118 (2003) 342.
25. X.-j. Wu, X.-j. Zhu, G.-y. Cao, and H.-y. Tu. *Simulation Modelling Practice and Theory*, 16 (2008) 494.
26. X.-J. Wu, X.-J. Zhu, G.-Y. Cao, and H.-Y. Tu. *J. Power Sources* 179 (2008) 232.
27. J. Yang, X. Li, H.-G. Mou, and L. Jian. *J. Power Sources*, 188 (2009) 475.
28. X.W. Zhang, S.H. Chan, H.K. Ho, J. Li, G. Li, and Z. Feng. *Int. J. Hyd. Energ*. 33 (2008) 2355.
29. S. Campanari, P. Iora. *J. Power Sources*, 132 (2004) 113.
30. D.J. Hall. Ph.D. Thesis, University of Pittsburgh, Pittsburgh, PA.
31. S.H. Chan, K. A. Khor, Z. T. Xia. J. Power Sources, 93(2011) 130.
32. A. Rezazadeh, A. Askarzadeh, M. Sedighizadeh. *Int. J. Electrochem. Sci*., 6 (2011) 3105.
33. M. ELSayed Youssef, Khairia E.AL-NAdi, Moataz H.Khalil. *Int. J. Electrochem. Sci.,* 5 (2010) 267.